Real-time Probing of an Atmospheric Photochemical Reaction by Ultrashort Extreme Ultraviolet Pulses: Nitrous Acid Release from *o*-Nitrophenol

Yuki Nitta[1], Oliver Schalk[2], Hironori Igarashi[1], Satoi Wada[3], Takuro Tsutsumi[3], Kenichiro Saita[3,4], Tetsuya Taketsugu[4,5], and Taro Sekikawa[1]

[1]Department of Applied Physics, Hokkaido Univ., Kita 13 Nishi 8, Kita-ku, Sapporo 060-8628, Japan

[2]Department of Chemistry, University of Copenhagen, Universitetsparken 5, DK-2100 Copenhagen, Denmark,

[3] Graduate School of Chemical Sciences and Engineering, Hokkaido Univ., Kita 10 Nishi 8, Kita-ku, Sapporo 060-0810, Japan

[4] Department of Chemistry, Hokkaido Univ., Kita 10 Nishi 8, Kita-ku, Sapporo 060-0810, Japan

[5] Institute for Chemical Reaction Design and Discovery (WPI-ICReDD), Hokkaido University, Sapporo 001-0021, Japan

Corresponding Author

sekiakwa@eng.hokudai.ac.jp

ABSTRACT. Photolysis of *o*-nitrophenol, contained in brown carbon, is considered to be a major process for the generation of nitrous acid (HONO) in the atmosphere. In this letter, we used time-resolved photoelectron spectroscopy with 29.5-eV probe pulses and ab initio calculations to disentangle all reaction steps from the excitation to the dissociation of HONO. After excitation, ultrafast excited state intramolecular hydrogen transfer is followed by intersystem crossing to the triplet manifold, where the molecules deplanarizes and finally splits off HONO after 0.5-1 ps.

TOC GRAPHICS

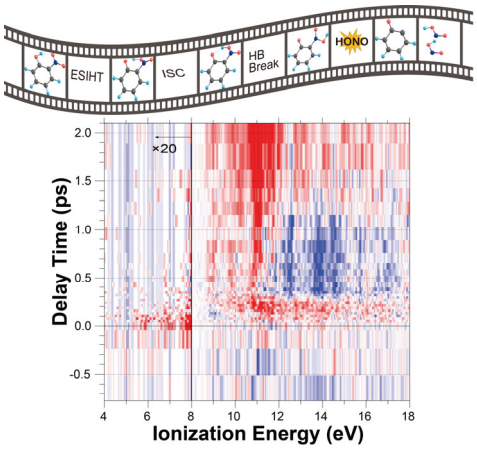

KEYWORDS. Time-resolved photoelectron spectroscopy, brown carbon, photolysis, excited-state intramolecular hydrogen transfer, intersystem crossing.

Nitrophenols (NPs) are produced by the combustion of wood or coal and are widely distributed in the gas phase and in organic aerosols in the atmosphere.[1-6] NPs absorb sunlight and are photoreactive.[5, 6]Their photolysis is considered as a source of nitrous acid (HONO).[7, 8] HONO is known for early-morning photochemical generation of OH radicals,[9-11] which are responsible for ozone formation and photochemical smog.[12] Therefore, NPs can be considered as a key pollutant, whose photochemistry needs to be understood. In particular, *o*-NP is of immense interest because its two main product channels upon photolysis are HONO and OH radicals[6, 8, 13] with almost wavelength independent quantum yields of 0.39 ± 0.07 and 0.70 ± 0.07 at 351 nm, and 0.34 ± 0.09 and 0.69 ± 0.07 at 308 nm, respectively.[6] Absorption spectrum of *o*-NP [14] is shown in the supporting information (SI).

The relaxation and photolysis processes of *o*-NP have been investigated with several approaches. Takezaki et al. reported that excited *o*-NP is likely to relax to the triplet manifold using time-resolved transient grating.[15] Ernst et al. investigated the relaxation dynamics of *o*-NP in both gaseous and liquid phases using time-resolved photoelectron spectroscopy (TRPES) and transient absorption spectroscopy using ultraviolet (UV) and visible laser pulses and suggested HONO dissociation to occur from the triplet state although they did not follow triplet state dynamics.[16] Ciavardini et al. observed the relaxation from the S_4 state by TRPES using 23.1-eV pulses[17] and identified two decay channels: Excited state intramolecular hydrogen transfer (ESIHT) and OH rotation. These experimental investigations were sensitive for the dynamics of the excited singlet states so that neither HONO nor OH radicals were observed. Theoretical studies predicted a more complicated process.[13, 18, 19] Xu et al. carried out ab initio molecular dynamics (AIMD) simulations after vertical excitation to the S_1 state and proposed three relaxation processes via the T_1 state: non-hydrogen transfer on a timescale of 300 fs, tunneling hydrogen transfer on a timescale of 10

ps, and direct hydrogen transfer on a timescale of 40 fs.[19] However, the experimental verification has not been demonstrated so far.

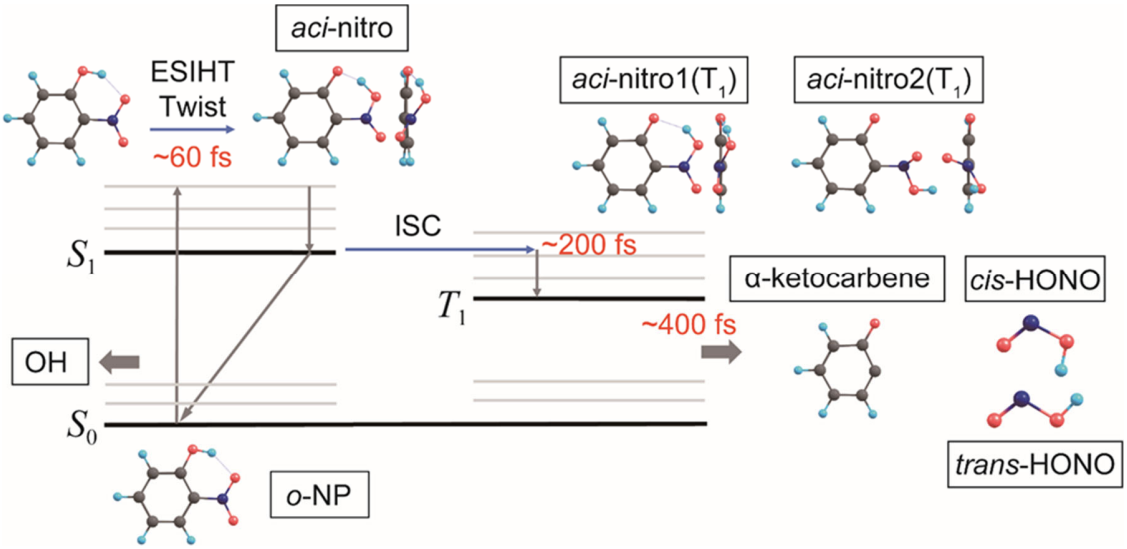

Figure 1. Relaxation and photolysis processes of *o*-NP with key intermediate states. Theoretical ionization energies and Cartesian coordinates are tabulated in SI.

In this paper, we investigate the relaxation and dissociation dynamics of *o*-NP using extreme ultraviolet (EUV) light at 29.5 eV[20-24] as a probe to reveal the complete photochemical dissociation pathway : 1) We were able to follow the dynamics from the Franck-Condon region to product formation by TRPES upon excitation at 400 nm (3.1 eV). 2) We used multireference perturbation theory, including both non-dynamical and dynamical electron correlation, to follow the reaction processes on the excited-state potential energy surfaces and to support experimental findings. We determined the ionization energies of *o*-NP in the ground and the intermediate reaction states with density functional theory (DFT) based on Koopmans' theorem. For the highest occupied molecular orbital (HOMO), we employed the vertical ionization energy calculated by the ΔSCF method

because it provides the ionization energy without any assumptions. The relaxation dynamics, proposed and discussed in this paper, is summarized in Fig. 1 including the structures of key intermediates. Details of the experimental and theoretical methods are provided in the SI.

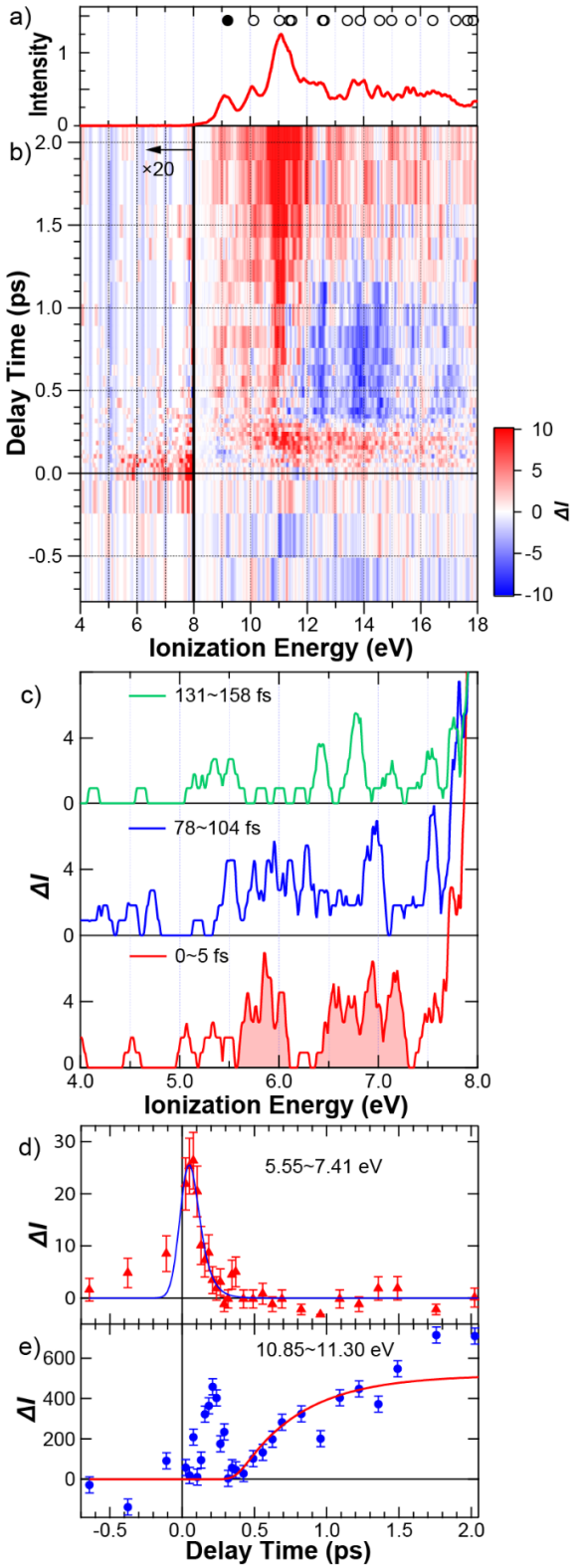
a)
Intensity
b)
×20
Delay Time (ps)
Ionization Energy (eV)
ΔI
c)
131~158 fs
78~104 fs
0~5 fs
ΔI
Ionization Energy (eV)
d)
5.55~7.41 eV
ΔI
e)
10.85~11.30 eV
ΔI
Delay Time (ps)

Figure 2. a) Photoelectron spectrum of *o*-NP in the ground state. Open circles indicate the absolute values of MO energies calculated by DFT except for the HOMO. The solid circle is the ionization energy calculated by the ΔSCF method. b) Difference photoelectron (ΔI) spectrogram. Below 8 eV, ΔI is magnified by a factor of 20. c) Temporal evolution of the photoelectron spectrum between 4.0 and 8.0 eV integrated between 0 and 5 fs (lower), 78 and 104 fs (middle), and 131 and 158 fs (upper). d) and e) Time dependences of photoelectron yields between 7.41 and 5.55 eV (▲) and between 11.30 and 10.85 eV (●), respectively. The solid lines are the results of fitting.

Figure 2a shows the photoelectron spectrum of *o*-NP as measured with the probe pulse only, which is consistent with previous reports.[25] The circles in Fig. 2a indicate the theoretical ionization energies calculated by DFT (see SI for detail), which agree with the experimental results. Figure 2b shows the difference photoelectron spectrum (ΔI) where the signal before time zero was subtracted from the measured signal. Three main features were observed: i) the appearance of excited states between 5 and 8 eV, ii) the appearance of the transient states around 250 fs with short lifetimes after the pump pulse in the energy region between 10 and 17 eV, and iii) a gradual increase in the intensity of the photoelectron band around 11 eV after 400 fs.

In the following, we discuss these features one by one. First, we focus on the excited states. Since the pump pulse has an energy of 3.1 eV and the vertical ionization potential is 9.1 eV, the ionization cut-off for the S_1 state is expected at approximately 6 eV. Figure 2c shows the temporal evolution of the photoelectron spectrum in the region of the excited states. At time zero, two bands appear around 5.9 and 7.0 eV shown by the red-shaded area. Those can be assigned to ionization to the two lowest lying ionic states which are separated by ~1.1 eV. Between 78 and 104 fs, the two bands merge to a single band. Since ESIHT is expected to be the first relaxation process, [16, 19] we attribute this band to the singlet excited state of the *aci*-nitro form (see Fig. 1), in agreement

with previous studies.[26, 27] A plot of the photoelectron yield between 5.50 and 7.41 eV is shown in Fig. 2d. The dynamics of the excited states can be represented by a single exponential decay function with a time constant of τ_{10}= (60 ± 16) fs convoluted with a Gaussian response function with a width of τ_{400nm} of 130 fs. This time constant is supposed to include singlet excited state processes, i.e. ESIHT and ISC to the triplet state or internal conversion back to the ground state. Due to the weak signal, we cannot reliably fit the data energy resolved, but we consider the results to agree roughly with the 130 ± 10 fs obtained in Ref. 16 and the rise time of the signal in the 10-17 eV region (see below).

To complement our experimental results, ab initio calculations were performed at the complete active space second-order perturbation theory (CASPT2) level based on the state-averaged CAS self-consistent field (SA-CASSCF) wavefunction, using the Sapporo-DZP-2012 basis set.[28] At the CASPT2/SA-CASSCF(8,7) level (the seven orbitals in the active space contain two π, two n, and three π* orbitals), the S_1 state of *o*-NP has ππ* excitation character in the Franck–Condon region and has an excitation energy of 4.04 eV which is in good agreement with the lowest lying peak of the absorption spectrum at 3.67 eV, while the S_2 state has nπ* excitation character at 4.27 eV. This is consistent with a previous study that involved time-dependent density functional theory (TDDFT) and second-order approximate coupled cluster (CC2) calculations,[29] but contradicts SA-CASSCF calculations which predicted an nπ* character of the S_1 state.[18, 19]

We further calculated the reaction pathway along the meta-intrinsic reaction coordinate (meta-IRC) from the Franck–Condon geometry at the CASPT2/SA3-CASSCF(4,4) level (four electrons in four orbitals of two π and two π* in the active space with three singlet states averaged) by the global reaction route mapping program, GRRM17.[30] Figure 3 shows (a) variations of the potential energies of the S_0 and S_1(ππ*) state and (b) variations of two interatomic distances (r_{O1H2}, r_{O3H2}),

which show the transition of the hydrogen atom during ESIHT, and two dihedral angles ($d_{O3N5C6C7}$, $d_{O4N5C6C8}$), which indicate the twist of the ONOH group with respect to the aromatic ring (after ESIHT) along the meta-IRC from the Franck–Condon point in the S_1 state, with (c) the molecular structures at s = 0.0, 1.6, and 5.6 Å amu$^{1/2}$, where s denotes the reaction coordinate. In the first step, a H atom (H2, see Figure 3c for atom labeling) is gradually transferred from O1 to O3 (s = 0–1.6). This reaction occurs barrierless and with a steep gradient. Then, the ONOH group starts to rotate about the C–N bond until the dihedral angle, $d_{O4N5C6C8}$, reaches approximately 45°. This twisting motion does not experience a steep gradient and dynamics are considered to be slower than for the ESHIT. A similar twist of the ONOH moiety was reported before.[16]

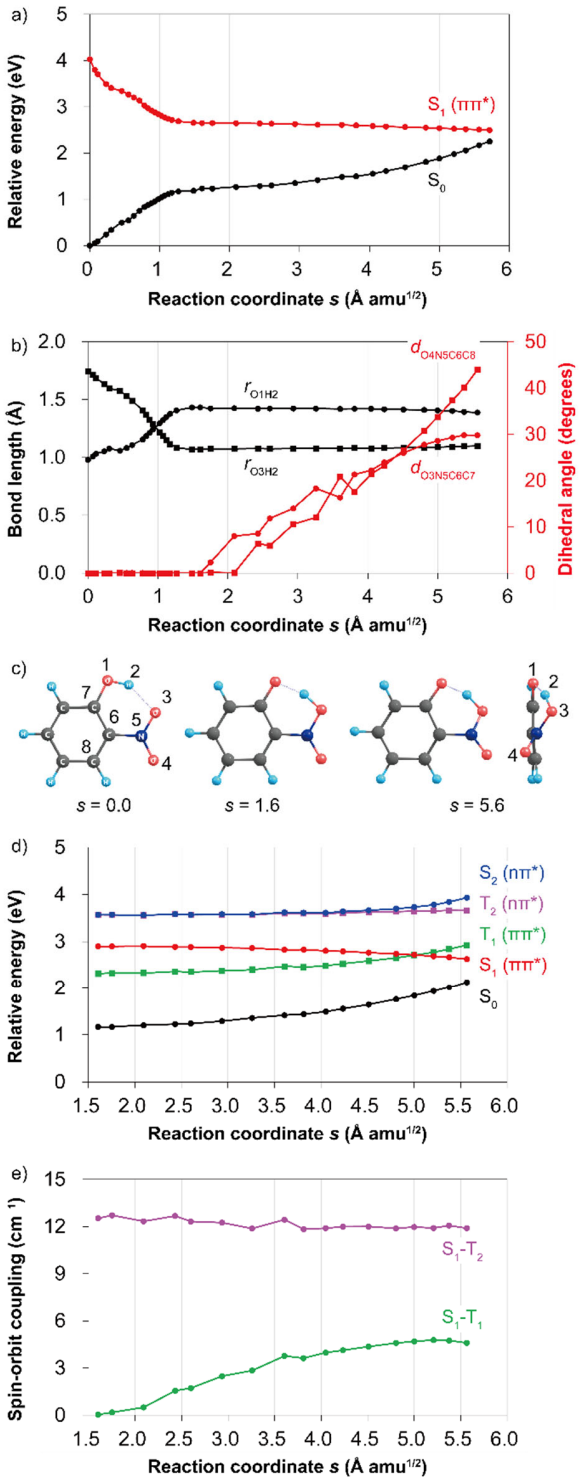

Figure 3. a) Potential energies of the S_0 and $S_1(\pi\pi^*)$ state and (b) variations of two interatomic distances (r_{O1H2}, r_{O3H2}) and two dihedral angles ($d_{O3N5C6C7}$, $d_{O4N5C6C8}$) along the reaction pathway

from the Franck–Condon point in the S_1 state, with (c) the molecular structures at s = 0.0, 1.6, and 5.6 Å amu$^{1/2}$, where s denotes a reaction coordinate at the CASPT2/SA3-CASSCF(4,4) level. d) Energy profiles of S_0, $S_1(\pi\pi^*)$, $S_2(n\pi^*)$, $T_1(\pi\pi^*)$, and $T_2(n\pi^*)$ states at the CASPT2/SA9-CASSCF(8,7) level and (e) SOCs between $S_1(\pi\pi^*)$ and $T_1(\pi\pi^*)$ and between $S_1(\pi\pi^*)$ and $T_2(n\pi^*)$ by the SA9-CASSCF(8,7) method along the reaction pathway in the region $s \geq 1.6$ Å amu$^{1/2}$.

After ESIHT in the $S_1(\pi\pi^*)$ state, HONO dissociation may hypothetically occur in the S_0, S_1 or the triplet states. To investigate whether ISC is possible, we calculated the energy variations of the T_1 and T_2 states and the spin–orbit coupling (SOC) between the S_1 and T_1 and T_2 states along the meta-IRC at $s \geq 1.6$ Å amu$^{1/2}$. The characters of the T_1 and the T_2 state are $\pi\pi^*$ and $n\pi^*$ in the Franck-Condon region, respectively. Figure 3d shows that the T_1 state lies close to the S_1 state along the reaction pathway, and their potential energy curves are isoenergetic at s = 5 near the S_1 minimum. While the SOC between $S_1(\pi\pi^*)$ and $T_1(\pi\pi^*)$ is almost zero for a planar geometry, [31, 32] the twisted NO_2H moiety leads to a change in character and the SOC is no longer zero, which renders ISC possible (see Fig. 3e). Under consideration of the quantum yield of HONO,[6] we infer that ~30% of the singlet *aci*-nitro form might cross from S_1 into T_1 and that the rest of the population eventually returns to the hot ground state of *o*-NP from where OH is dissociated.

In the region between 10 and 17 eV, a transient band appears with the approximate decay time of the (singlet) excited state signal and reaches a maximum at around 250 fs. This rise (and the subsequent decay) could not be fitted with an exponential function which can be explained by the highly non-exponential behavior of the dynamics. This means that the time frame of the dynamics is not dominated by a statistical transition between two states rather than by the time the molecules needs to complete the subsequent steps of the reaction process. Exemplarily for the dynamics, the temporal evolution between 10.85 and 11.30 eV is shown in Fig. 2e. In order to describe the

progression of the dynamics in more detail, consider the difference spectra at 184 and 403 fs shown in Figures 4c and 4e, respectively, together with the photoelectron spectrum of *o*-NP in Fig. 4a. The most prominent difference of the spectra is the absence of the band at 8.8 eV at 184 fs, while this band is present at 403 fs. To evaluate this feature, we used spin-unrestricted DFT calculations with the ωB97XD functional to find two nonplanar minimum structures in the T_1 state, *aci*-nitro1 and *aci*-nitro2, whose structures and theoretical ionization energies are shown in Fig. 1 and Figs. 4b and 4d, respectively (see SI for details). In *aci*-nitro1, the hydrogen bond is retained; whereas the HONO group is twisted and the hydrogen bond is broken in *aci*-nitro2. The most notable difference between these structures is the absence of MOs between 8.0 and 9.5 eV for *aci*-nitro1 (see Figs. 4b and 4d, where α and β denote the electron spin). Hence, we propose that, after ESIHT, the molecular geometry changes from the twisted *aci*-nitro (S_1 state) to *aci*-nitro1 (T_1 state) through the S_1–T_1 transition region at $s = 5$ (see Fig. 3d) and then transforms to *aci*-nitro2 by ~400 fs, from which HONO can dissociate.

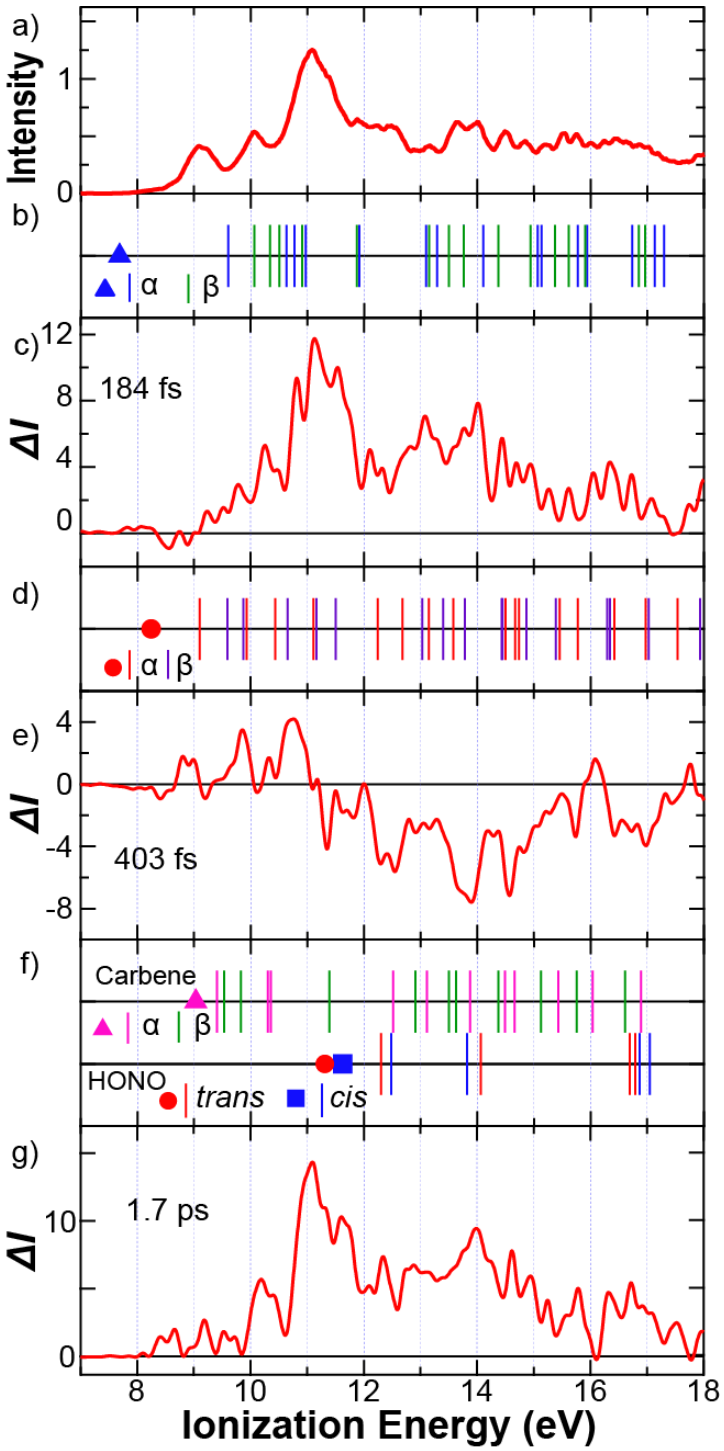
a)
Intensity
1
0
b)
α
β
c)
12
8
4
0
ΔI
184 fs
d)
α
β
e)
4
0
-4
-8
ΔI
403 fs
f)
Carbene
α
β
HONO
trans
cis
g)
10
0
ΔI
1.7 ps
8
10
12
14
16
18
Ionization Energy (eV)

Figure 4. a) Photoelectron spectrum of *o*-NP in the ground state. b) and d) Calculated ionization energies of *aci*-nitro1 and *aci*-nitro2, respectively. c) and e) Difference photoelectron spectra at 184 and 403 fs, respectively. f) Calculated ionization energies of α-ketocarbene in the triplet state (carbene) and *trans*- and *cis*-HONO in the singlet state. g) Difference spectrum at 1.7 ps, subtracted from the spectrum at 400 fs. The solid marks in b), d), and f) are the ionization energies calculated by the ΔSCF method. Vertical lines indicate the absolute values of MO energies except for the HOMOs.

Figure 2b shows an increase of the band around 11 eV between 0.5 and 2.0 ps. To visualize the spectral change after 400 fs, the difference spectrum between 1.7 ps and 400 fs is shown in Fig. 4g. We propose that these spectral changes are caused by HONO dissociation. This is evidenced by the calculation of the ionization spectrum of α-ketocarbene (carbene) in the triplet state and of *trans*- and *cis*-HONO in the singlet state (see Fig. 1). They are plotted in Fig. 4f. The characteristic peaks at 11.1, 11.6, 12.3, and 14.0 eV in the spectrum at 1.7 ps are consistent with the calculations for HONO. In addition, the peak at 10.1 eV can be attributed to α-ketocarbene. This assignment is also supported by the experimental photoelectron spectrum of HONO in Ref. 33.

The temporal evolution of the 11-eV band integrated between 10.85 and 11.30 eV for HONO production is plotted in Fig. 2e. After the cleavage of the hydrogen bond in the triplet state at approximately 400 fs, the band begins to increase gradually with a single exponential rise time of 433 ± 227 fs starting at 374 ± 97 fs after time zero. (see SI for detail)

In previous studies, the photochemical production of OH radicals was reported.[6, 13, 34] If OH radicals were directly produced by the photolysis of *o*-NP, the photoelectrons from OH radicals should be detected at an ionization energy of 13.01 eV.[35] However, no isolated peak at

approximately 13 eV was identified. As a consequence, OH radicals must be produced thermally from the hot ground state of *o*-NP.

In conclusion, we were able to follow the full photodissociation processes of *o*-NP from the Franck–Condon region to the release of HONO. This was possible by the use of a high harmonic light source which enabled us to access not only the singlet states (as in UV probe photoelectron spectroscopy) but also the triplet state and the ground state of the photoproducts.

ASSOCIATED CONTENT

Supporting Information

The Supporting Information is available free of charge.

Experimental methods, including the cross-correlation traces between the pump (=3.1 eV) and probe (=29.5 eV) pulses and the absorption spectrum of *o*-nitrophenol. Table of Cartesian coordinates of optimized structures and theoretical ionization energies by density functional theory (DFT) calculations with the ωB97XD functional and with the Sapporo-DZP-2012+diffuse(sp) basis set.

Corresponding Author

Taro Sekikawa

Department of Applied Physics, Hokkaido Univ., Kita 13 Nishi 8, Kita-ku, Sapporo 060-8628,

Japan; E-mail: sekikawa@eng.hokudai.ac.jp

Notes

The authors declare no competing financial interests.

ACKNOWLEDGMENT

TS is financially supported by MEXT Q-LEAP (JPMXS0118068681), JST CREST (JPMJCR15N1), and KAKENHI(19H01814). TT thanks to a grant from the Photo-excitonix

Project in Hokkaido University and JST CREST (JPMJCR1902). Some of calculations were performed using the Research Center for Computational Science, Okazaki, Japan.

REFERENCES

1. Nojima, K.; Kawaguchi, A.; Ohya, T.; Kanno, S.; Hirobe, M., Studies on photochemical reaction of air pollutants. X. Identification of nitrophenols in suspended particulates. *Chem. Pharm. Bull.* **1983,** *31*, 1047-1051.
2. Leuenberger, C.; Ligocki, M. P.; Pankow, J. F., Trace organic compounds in rain. 4. Identities, concentrations, and scavenging mechanisms for phenols in urban air and rain. *Environ. Sci. Tech.* **1985,** *19*, 1053-1058.
3. Tremp, J.; Mattrel, P.; Fingler, S.; Giger, W., Phenols and nitrophenols as tropospheric pollutants: Emissions from automobile exhausts and phase transfer in the atmosphere. *Water, Air, and Soil Pollution* **1993,** *68*, 113-123.
4. Lüttke, J.; Scheer, V.; Levsen, K.; Wünsch, G.; Cape, J. N.; Hargreaves, K. J.; Storeton-West, R. L.; Acker, K.; Wieprecht, W.; Jones, B., Occurrence and formation of nitrated phenols in and out of cloud. *Atmos. Environ.* **1997,** *31*, 2637-2648.
5. Hinrichs, R. Z.; Buczek, P.; Trivedi, J. J., Solar absorption by aerosol-bound nitrophenols compared to aqueous and gaseous nitrophenols. *Environ. Sci. Technol.* **2006,** *50*, 5661-5667.
6. Sangwan, M.; Zhu, L., Absorption cross sections of 2-nitrophenol in the 295−400 nm region and photolysis of 2-nitrophenol at 308 and 351 nm. *J. Phys. Chem. A* **2016,** *120*, 9958-9967.
7. Barsotti, F.; Bartels-Rausch, T.; Laurentiis, E. D.; Ammann, M.; Brigante, M.; Mailhot, G.; Maurino, V.; Minero, C.; Vione, D., Photochemical formation of nitrite and nitrous acid (hono) upon irradiation of nitrophenols in aqueous solution and in viscous secondary organic aerosol proxy. *Environ. Sci. Tech.* **2017,** *51*, 7486−7495.
8. Bejan, I.; Aal, Y. a. E.; Barnes, I.; Benter, T.; Bohn, B.; Wiesena, P.; Kleffmann, J., The photolysis of ortho-nitrophenols: A new gas phase source of hono. *Phys. Chem. Chem. Phys.* **2006,** *8*, 2028–2035.
9. Stutz, J.; Kim, E. S.; Platt, U.; Bruno, P.; Perrino, C.; Febo, A., Uv‐visible absorption cross sections of nitrous acid. *J. Geophys. Res.* **2000,** *105*, 14585-14592.
10. Li, X.; Rohrer, F.; Hofzumahaus, A.; Brauers, T.; Häseler, R.; Bohn, B.; Broch, S.; Fuchs, H.; Gomm, S.; Holland, F.; Jäger, J.; Kaiser, J.; Keutsch, F. N.; Lohse, I.; Lu, K.; Tillmann, R.; Wegener, R.; Wolfe, G. M.; Mentel, T. F.; Kiendler-Scharr, A.; Wahner, A., Missing gas-phase source of hono inferred from zeppelin measurements in the troposphere. *Science* **2014,** *344*, 292-296.
11. Sangwan, M.; Zhu, L., Role of methyl-2-nitrophenol photolysis as a potential source of oh radicals in the polluted atmosphere: Implications from laboratory investigation. *J. Phys. Chem. A* **2018,** *122*, 1861−1872.
12. Gligorovski, S.; Strekowski, R.; Barbati, S.; Vione, D., Environmental implications of hydroxyl radicals (•oh). *Chem. Rev.* **2015,** *24*, 13051–13092.
13. Cheng, S.-B.; Zhou, C.-H.; Yin, H.-M.; Sun, J.-L.; Han, K.-L., Oh produced from o-nitrophenol photolysis: A combined experimental and theoretical investigation. *J. Chem. Phys.* **2009,** *130*, 234311.

14. Chen, J.; Wenger, J. C.; Venables, D. S., Near-ultraviolet absorption cross sections of nitrophenols and their potential influence on tropospheric oxidation capacity. *J. Phys. Chem. A* **2011,** *115*, 12235-12242.
15. Takezaki, M.; Hirota, N.; Terazima, M., Nonradiative relaxation processes and electronically excited states of nitrobenzene studied by picosecond time-resolved transient grating method. *J. Phys. Chem. A* **1997,** *101*, 3443-3448.
16. Ernst, H. A.; Wolf, T. J. A.; Schalk, O.; González-García, N.; Boguslavskiy, A. E.; Stolow, A.; Olzmann, M.; Unterreiner, A.-N., Ultrafast dynamics of o-nitrophenol: An experimental and theoretical study. *J. Phys. Chem. A* **2015,** *119*, 9225-9235.
17. Ciavardini, A.; Coreno, M.; Callegari, C.; Spezzani, C.; Ninno, G. D.; Ressel, B.; Grazioli, C.; Simone, M. D.; Kivimäki, A.; Miotti, P.; Frassetto, F.; Poletto, L.; Puglia, C.; Fornarini, S.; Pezzella, M.; Bodo, E.; Piccirillo, S., Ultra-fast-vuv photoemission study of uv excited 2-nitrophenol. *J. Phys. Chem. A* **2019,** *123*, 1295-1302.
18. Xu, C.; Yu, L.; Zhu, C.; Yu, J., Photoisomerization reaction mechanisms of o-nitrophenol revealed by analyzing intersystem crossing network at the mrci level. *J. Phys. Chem. A* **2015,** *119*, 10441-10450.
19. Xu, C.; Yu, L.; Zhu, C.; Yu, J.; Cao, Z., Intersystem crossing-branched excited-state intramolecular proton transfer for o-nitrophenol: An ab initio on-the-fly nonadiabatic molecular dynamic simulation. *Sci. Rep.* **2016,** *6*, 26768.
20. Iikubo, R.; Fujiwara, T.; Sekikawa, T.; Harabuchi, Y.; Satoh, S.; Taketsugu, T.; Kayanuma, Y., Time-resolved photoelectron spectroscopy of dissociating 1,2-butadiene molecules by high harmonic pulses. *J. Phys. Chem. Lett.* **2015,** *6* (13), 2463-2468.
21. Iikubo, R.; Sekikawa, T.; Harabuchi, Y.; Taketsugu, T., Structural dynamics of photochemical reactions probed by time-resolved photoelectron spectroscopy using high harmonic pulses. *Faraday Discuss.* **2016,** *194*, 147-160.
22. Makida, A.; Igarashi, H.; Fujiwara, T.; Sekikawa, T.; Harabuchi, Y.; Taketsugu, T., Ultrafast relaxation dynamics in trans-1,3-butadiene studied by time-resolved photoelectron spectroscopy with high harmonic pulses. *J. Phys. Chem. Lett.* **2014,** *5* (10), 1760-1765.
23. Ito, M.; Kataoka, Y.; Okamoto, T.; Yamashita, M.; Sekikawa, T., Spatiotemporal characterization of single-order high harmonic pulses from time-compensated toroidal-grating monochromator. *Opt. Express* **2010,** *18*, 6071-6078.
24. Igarashi, H.; Makida, A.; Ito, M.; Sekikawa, T., Pulse compression of phase-matched high harmonic pulses from a time-delay compensated monochromator. *Opt. Express* **2012,** *20* (4), 3725-3732.
25. Kobayashi, T.; Nagakura, S., Photoelectron spectra of nitrophenols and nitroanisoles. *J. Electron Spectrosc. Relat. Phenom.* **1975,** *6*, 421-427.
26. Wang, Y.-Q.; Wang, H.-G.; Zhang, S.-Q.; Pei, K.-M.; Zheng, X., Resonance raman intensity analysis of the excited state proton transfer dynamics of 2-nitrophenol in the charge-transfer band absorption. *J. Chem. Phys.* **2006,** *125*, 214506.
27. Nakata, A.; Tsuneda, T., Density functional theory for comprehensive orbital energy calculations. *J. Chem. Phys.* **2013,** *139*, 064102.
28. Noro, T.; Sekiya, M.; Koga, T., Segmented contracted basis sets for atoms h through xe: Sapporo-(dk)-nzp sets (n = d, t, q). *Theoretical Chemistry Accounts* **2012,** *131*, 1124.
29. Guthmuller, J., Assessment of td-dft and cc2 methods for the calculation of resonance raman intensities: Application to o-nitrophenol. *J. Chem. Theory Comput.* **2011,** *7*, 1082-1089.

30. Maeda, S.; Harabuchi, Y.; Sumiya, Y.; Takagi, M.; Suzuki, K.; Hatanaka, M.; Osada, Y.; Taketsugu, T.; Morokuma, K.; Ohno, K. *Grrm17*, http://iqce.jp/GRRM/index_e.shtml (accessed date 25 September 2020).
31. Baba, M., Intersystem crossing in the $^1n\pi^*$ and $^1\pi\pi^*$ states. *J. Phys. Chem. A* **2011,** *115*, 9514-9519.
32. El‐Sayed, M. A., Spin−orbit coupling and the radiationless processes in nitrogen heterocyclics. *J. Chem. Phys.* **1963,** *38*, 2834-2838.
33. Wang, W.; Ge, M.; Yao, L.; Zeng, X.; Wang, Z., A novel heterogeneous reaction for generating gaseous nitrous acid. *Chin. Sci. Bull.* **2007,** *52*, 3056-3060.
34. Wei, Q.; Yin, H.-M.; Sun, J.-L.; Yue, X.-F.; Han, K.-L., The dynamics of oh channel in the 266 and 355 nm photodissociation of 2-nitrophenol. *Chem. Phys. Lett.* **2008,** *463*, 340–344.
35. Van Lonkhuyzen, H.; De Lange, C. A., U.V. Photoelectron spectroscopy of oh and od radicals. *Mol. Phys.* **1984,** *51*, 551-568.